Hybrid Model Predictive Control for Fully Electric Vehicle Thermal Management System Optimal Mode Selection

Jan Glos, František Šolc, Lukáš Otava, Pavel Václavek

J. Glos, F. Šolc, L. Otava and P. Václavek, "Hybrid Model Predictive Control for Fully Electric Vehicle Thermal Management System Optimal Mode Selection," IECON 2020 The 46th Annual Conference of the IEEE Industrial Electronics Society, Singapore, Singapore, 2020, pp. 2036-2043.

DOI: 10.1109/IECON43393.2020.9254286

IEEE Xplore: ieeexplore.ieee.org

Hybrid Model Predictive Control for Fully Electric Vehicle Thermal Management System Optimal Mode Selection

Jan Glos*, František Šolc†, Lukáš Otava‡, Pavel Václavek§
CEITEC - Central European Institute of Technology
Brno University of Technology
Brno, Czech Republic
* ORCID ID 0000-0001-9636-1529, † Email: frantisek.solc@ceitec.vutbr.cz,
‡ ORCID ID 0000-0003-2442-816X, § ORCID ID 0000-0001-8624-5874

***Abstract*—Vehicle thermal management systems of Fully Electric Vehicles bring increased demands on control algorithms to operate the vehicle efficiently. Especially, if there are multiple heat sources and sinks (cabin, batteries, electric drive, thermal energy storage, etc.), it is necessary to select the system operating mode (configuration of actuators), under which the system will operate efficiently with respecting defined constraints and references tracking. This paper brings a novel approach to the decision-making algorithm, which is based on the Hybrid Model Predictive Control and optimally solves the problem with regards to the defined objective function.**

***Index Terms*—vehicle thermal management system, VTMS, model predictive control, MPC, hybrid model predictive control, HMPC, piecewise-affine, PWA, thermal energy storage, TES, heat pump, fully electric vehicle, FEV, vapor compression refrigeration system, VCRS, waste heat recovery, decision-making algorithm**

I. Introduction

Fully electric vehicles (FEV) are getting more widely used in individual transport systems, but they are still facing several issues, which complicate their usage. One of them is their weather-dependent range, which means that under cold ambient temperatures the range of vehicles dramatically decreases [1] down to less than half of their nominal range. This issue partially depends on increased high-voltage (HV) battery internal resistance under cold conditions [2]. Secondly, this issue is caused also by Heating, Ventilation, and Air Conditioning (HVAC) system, which needs to be powered from HV battery. Especially the cabin heating can decrease the vehicle range by $\sim 20\,\%$ at an ambient temperature of $-7\,^{\circ}\mathrm{C}$ [3] and even worse for lower temperatures.

The issues described above are related not only with FEV but also hybrid electric vehicles (HEV) does not have enough waste heat for cabin heating [4], what leads to a continuous run of the internal combustion engine (ICE) and thus inefficient vehicle operation or insufficient passenger comfort due to low cabin temperature.

The issue does not have a single and simple solution, but there are several approaches, which can reduce the negative impact of low ambient temperatures, e.g. heat pump systems, waste heat recovery, insulation, thermal energy storage (TES), preconditioning and others. On top of them stands a vehicle thermal management system (VTMS) design, which interconnects the parts in a vehicle and, if properly proposed, can substantially help to avoid energy losses. For particular VTMS we can find operating modes (also called thermal functions), which define the behavior of VTMS components (e.g. heating by heat pump, heating by an electric resistive heater, cooling by ambient air, cooling by the refrigeration system, etc.). Each manufacturer and OEM has a slightly different VTMS approach [5], but all of them have one common challenge: control and especially real-time decision-making control system. Its task is to select the VTMS operating mode in such a way, that the vehicle will operate efficiently, constraints (HV battery temperature, powertrain temperatures, etc.) will be fulfilled and the references (e.g. cabin temperature) will be achieved.

This problem can be solved by various techniques, the most simple will employ heuristic knowledge implemented in the form of the state diagram. This approach was tested by us and it was found that the implementation requires an excessive number of constants, thresholds, safety functions, and the system is hard to tune. Moreover, each change in VTMS leads to a complete redesign of a state diagram and it is also hard to determine if the system operates efficiently and optimally.

As the heuristic method is not fully suitable for this task, we tried to find a way of more general and objectively optimal decision-making system. This paper presents one possible solution, which is based on a hybrid model predictive control (HMPC) designed using the thermo-electric high-level piecewise affine (PWA) model of VTMS.

II. Hybrid Model Predictive Control

In [6] it was shown that five classes of hybrid systems: mixed logical dynamical (MLD) systems, linear complementarity (LC) systems, extended linear complementarity (ELC) systems, piecewise affine (PWA) systems and max-min-plus-scaling (MMPS) systems are equivalent and the conversion between them is possible. Then it was shown in [7] that MLD systems can be successfully controlled by MPC and thus also

PWA and other hybrid systems can be controlled using this technique.

We will focus only on MLD and PWA systems, as the others are not interesting for this work. MLD system [8] is usually written as

$$\mathbf{x}_{k+1} = \mathbf{A}\mathbf{x}_k + \mathbf{B}_1\mathbf{u}_k + \mathbf{B}_2\boldsymbol{\delta}_k + \mathbf{B}_3\mathbf{z}_k, \tag{1}$$

$$\mathbf{y}_k = \mathbf{C}\mathbf{x}_k + \mathbf{D}_1\mathbf{u}_k + \mathbf{D}_2\boldsymbol{\delta}_k + \mathbf{D}_3\mathbf{z}_k, \tag{2}$$

$$\mathbf{E}_1\mathbf{x}_k + \mathbf{E}_2\mathbf{u}_k + \mathbf{E}_3\boldsymbol{\delta}_k + \mathbf{E}_4\mathbf{z}_k \leq \mathbf{g}, \tag{3}$$

where $\mathbf{x}_k = \begin{bmatrix}\mathbf{x}_k^{\mathrm{r}} & \mathbf{x}_k^{\mathrm{b}}\end{bmatrix}^\mathsf{T}$ is state vector consisting of real $\mathbf{x}_k^{\mathrm{r}} \in \mathbb{R}^{n_{\mathrm{r}}}$ and binary $\mathbf{x}_k^{\mathrm{b}} \in \{0,1\}^{n_{\mathrm{b}}}$ states. Input $\mathbf{u}_k$ and output $\mathbf{y}_k$ vectors have a structure similar to the state vector and $\mathbf{z}_k \in \mathbb{R}^{r_{\mathrm{r}}}$ and $\boldsymbol{\delta}_k \in \{0,1\}^{r_{\mathrm{b}}}$ are auxiliary variables.

PWA system can be described [9] by

$$\mathbf{x}_{k+1} = \mathbf{A}_i\mathbf{x}_k + \mathbf{B}_i\mathbf{u}_k + \mathbf{f}_i^{\mathrm{c}}, \tag{4}$$

$$\mathbf{y}_k = \mathbf{C}_i\mathbf{x}_k + \mathbf{D}_i\mathbf{u}_k + \mathbf{g}_i^{\mathrm{c}}, \tag{5}$$

$$\text{for } \begin{bmatrix}\mathbf{x}_k \\ \mathbf{u}_k\end{bmatrix} \in \boldsymbol{\Omega}_i, \tag{6}$$

where $\mathbf{x}_k \in \mathbb{R}^n$, $\mathbf{u}_k \in \mathbb{R}^m$, and $\mathbf{y}_k \in \mathbb{R}^l$ denote the states, inputs, and outputs vectors respectively. $\boldsymbol{\Omega}_i$ denotes convex polyhedra in the combined input-state space. $\mathbf{f}_i^{\mathrm{c}}$ and $\mathbf{g}_i^{\mathrm{c}}$ are constant vectors. The subscript $i \in \{1, 2 \dots s\}$ denotes the mode of the PWA system with s modes altogether.

The conversion between MLD and PWA is well described in [8]. If the PWA system is described in the format of (1)-(3), it can be easily incorporated into an objective function

$$J_N(\mathbf{x}_0, \boldsymbol{\Psi}) = \frac{1}{2}\boldsymbol{\Psi}^\mathsf{T}\mathbf{G}\boldsymbol{\Psi} + \mathbf{x}_0^\mathsf{T}\mathbf{F}^\mathsf{T}\boldsymbol{\Psi}, \tag{7}$$

$$\text{s.t.} \qquad \mathbf{S}_1\boldsymbol{\Psi} \leq \mathbf{S}_2 + \mathbf{S}_3\mathbf{x}_0, \tag{8}$$

where

$$\boldsymbol{\Psi} \triangleq \begin{bmatrix}\hat{\mathbf{u}}^\mathsf{T} & \hat{\boldsymbol{\delta}}^\mathsf{T} & \hat{\mathbf{z}}^\mathsf{T}\end{bmatrix}^\mathsf{T} \tag{9}$$

and the matrices $\mathbf{G}$, $\mathbf{F}$, $\mathbf{S}_1$, $\mathbf{S}_2$, and $\mathbf{S}_3$ are properly constructed from penalization and state prediction matrices.

The objective function can be then minimized using available solvers, as it is in the format of mixed-integer quadratic (constrained) programming (MIQP or MIQCP). For such a class of problems, the solvers are usually based on branch and bound method (used e.g. by GUROBI optimizer). This approach is only applicable to online (implicit) MPC.

The other option of PWA optimal control is the multiparametric method by Borelli in [10], which doesn't employ the transition of the PWA system to the MLD system but solves the optimization problem backward in time of prediction horizon. This approach is applicable for offline (explicit) MPC.

III. Decision Model Predictive Control

We propose to use MPC for selection of optimal control strategy of complex t-invariant nonlinear system

$$\mathbf{x}_{k+1} = \mathbf{f}(\mathbf{x}_k, \mathbf{u}_k), \tag{10}$$

$$\mathbf{y}_k = \mathbf{h}(\mathbf{x}_k, \mathbf{u}_k), \tag{11}$$

with $\mathbf{x}$, $\mathbf{u}$, and $\mathbf{y}$ being the vectors of states, inputs, and outputs, $\mathbf{f}(\cdot)$ state update function, and $\mathbf{h}(\cdot)$ the output function. Commonly, such a system has some binary $\mathbf{u}_k^{\mathrm{b}} \in \{0,1\}^{n_{\mathrm{b}}}$ and/or integral $\mathbf{u}_k^{\mathrm{i}} \in \mathbb{Z}^{n_{\mathrm{i}}}$ actuators (valves, switches, constant/step speed drives, etc.), which together forms modes of the system. Under these modes, the system is operated and possibly continuously controlled by continuous inputs $\mathbf{u}_k^{\mathrm{r}} \in \mathbb{R}^{n_{\mathrm{r}}}$. Usually, the switching between modes is somehow constrained (switching frequency, etc.). Then the input vector can be written as

$$\mathbf{u}_k = \begin{bmatrix}\mathbf{u}_k^{\mathrm{b}} \\ \mathbf{u}_k^{\mathrm{i}} \\ \mathbf{u}_k^{\mathrm{r}}\end{bmatrix}. \tag{12}$$

We assume that we can find a simplified model of such a system in the form of a general high-level PWA dynamic model (incorporating e.g. generalized thermal flows, material flows, electric power flows, etc.). We define domain $\mathbb{U}_i^{\mathrm{b}}$ of i^{th} binary input variable u_i^{b} as

$$u_i^{\mathrm{b}} \in \mathbb{U}_i^{\mathrm{b}} \triangleq \{0,1\} \tag{13}$$

and similarly the domain $\mathbb{U}_i^{\mathrm{i}}$ of i^{th} integral input variable u_i^{i} as

$$u_i^{\mathrm{i}} \in \mathbb{U}_i^{\mathrm{i}} \subset \mathbb{Z}, \tag{14}$$

with the assumption of reasonably constrained domains of integral variables. We then list all the binary and integral inputs combinations

$$\mathbf{M} = \prod_{i=1}^{n_{\mathrm{b}}} \mathbb{U}_i^{\mathrm{b}} \times \prod_{i=1}^{n_{\mathrm{i}}} \mathbb{U}_i^{\mathrm{i}} \tag{15}$$

and select their allowed combinations $\mathbf{M}_{\mathrm{a}} \subseteq \mathbf{M}$. Each item $m \in \mathbf{M}_{\mathrm{a}}$ is referred to as an *operating mode* and it is necessary to find an affine (or linear) dynamic description of the system within each operating mode. All the operating modes must have common vectors of inputs $\mathbf{u}^*$, states $\mathbf{x}^*$, and outputs $\mathbf{y}^*$, which, in general, will not be the same as the original vectors $\mathbf{u}$, $\mathbf{x}$, and $\mathbf{y}$ (they might be the same for simple systems). We suppose that all the operating modes share the same input and state constraints

$$\mathbf{E}\mathbf{x}_k^* + \mathbf{F}\mathbf{u}_k^* \leq \mathbf{G}, \tag{16}$$

which define the polyhedron

$$\mathcal{P} \subset \mathbb{R}^{n_{x^*}+n_{u^*}}. \tag{17}$$

Imagine that we succeed to find the dynamic description of i^{th} operating mode ($i = 1, 2 \dots |\mathbf{M}_{\mathrm{a}}|$) in affine form as

$$\mathbf{x}_{k+1}^* = \mathbf{A}_i\mathbf{x}_k^* + \mathbf{B}_i\mathbf{u}_k^* + \mathbf{f}_i^{\mathrm{c}}, \tag{18}$$

$$\mathbf{y}_k^* = \mathbf{C}_i\mathbf{x}_k^* + \mathbf{D}_i\mathbf{u}_k^* + \mathbf{g}_i^{\mathrm{c}}, \tag{19}$$

$$\text{for } \begin{bmatrix}\mathbf{x}_k^* \\ \mathbf{u}_k^*\end{bmatrix} \in \mathcal{P}_i, \tag{20}$$

then several possibilities can happen:

- $\mathcal{P}_i = \mathcal{P}$ or $\mathcal{P}_i \supset \mathcal{P}$, which means that the current operating mode is described by a single *PWA system mode*

- $\mathcal{P}_i \subset \mathcal{P}$, which means that there exist at least two operating submodes within the current operating mode

In the second case, we denote the polyhedron $\mathcal{P}_i$ as $\mathcal{P}_{i1}$ and we need to find an affine dynamic model for $\mathcal{P}_{i2} \triangleq \mathcal{P} \backslash \mathcal{P}_{i1}$. We repeat this step and stop the searching if the condition

$$\bigcup_{j=1}^{s_i} \mathcal{P}_{ij} \supseteq \mathcal{P} \tag{21}$$

is fulfilled, which means that the whole constrained state-input space is covered by s_i submodes models. Each submode then becomes a new *PWA system mode*. This procedure is repeated for each operating mode (i.e. i is incremented and we try to find a model within this operating mode using the steps above).

Example. *Submodes could be useful if we consider a nonlinear system with multiple functions (e.g. heating and cooling). We define two modes (for cooling and heating) and if the system has nonlinear behavior within the mode, it can be described by several submodes (obtained e.g. by linearization).*

The distinction between operating modes is proposed based on dummy input $\tilde{u}$, which denotes the item $m \in \mathbf{M}_\mathrm{a}$. The input $\tilde{u}$ can be defined as needed, we propose $\tilde{u} \in \mathbb{N}$ and to each operating mode value of $\tilde{u}$ is assigned, for i^{th} operating mode $\tilde{u} = i$.

The input $\tilde{u}$ is appended to PWA system input vector $\mathbf{u}^*$

$$\bar{\mathbf{u}} = \begin{bmatrix} \tilde{u} \\ \mathbf{u}^* \end{bmatrix} \tag{22}$$

and the polyhedron $\mathcal{P}$ has to be extended to

$$\mathcal{P}^* = \mathcal{P} \times \{1, 2 \dots |\mathbf{M}_\mathrm{a}|\}, \tag{23}$$

what is a polyhedral union of PWA system modes polyhedrons

$$\mathcal{P}^* = \bigcup_{i=1}^{|\mathbf{M}_\mathrm{a}|} \mathcal{P}_i^*, \tag{24}$$

where

$$\mathcal{P}_i^* = \begin{cases} \mathcal{P} \times i & \text{if } s_i = 1 \\ (\mathcal{P} \times i) \cap \bigcup_{j=1}^{s_i} \mathcal{P}_{ij}^* & \text{if } s_i > 1 \end{cases}, \tag{25}$$

where $i \in \{1, 2 \dots |\mathbf{M}_\mathrm{a}|\}$ and $\mathcal{P}_{ij}^* = \mathcal{P}_{ij} \times i$. For simplification of further text, we will denote $\mathcal{P}_i^*$ with no operating submodes as $\mathcal{P}_{i1}^*$. By recalling (4)-(6) and adjusting matrices $\mathbf{B}$ and $\mathbf{D}$ according to (22)

$$\mathbf{B}^* = \begin{bmatrix} \mathbf{0} & \mathbf{B} \end{bmatrix}, \qquad \mathbf{D}^* = \begin{bmatrix} \mathbf{0} & \mathbf{D} \end{bmatrix} \tag{26}$$

we get the description of the simplified system in PWA form

$$\mathbf{x}_{k+1}^* = \begin{cases} \mathbf{A}_{11}\mathbf{x}_k^* + \mathbf{B}_{11}^*\bar{\mathbf{u}}_k + \mathbf{f}_{11}^\mathrm{c} & \text{if } (\mathbf{x}_k^*, \bar{\mathbf{u}}_k) \in \mathcal{P}_{11} \\ \vdots & \vdots \\ \mathbf{A}_{|\mathbf{M}_\mathrm{a}|s_\mathrm{max}}\mathbf{x}_k^* + \mathbf{B}_{|\mathbf{M}_\mathrm{a}|s_\mathrm{max}}^*\bar{\mathbf{u}}_k + \mathbf{f}_{|\mathbf{M}_\mathrm{a}|s_\mathrm{max}}^\mathrm{c} & \text{if } (\mathbf{x}_k^*, \bar{\mathbf{u}}_k) \in \mathcal{P}_{|\mathbf{M}_\mathrm{a}|s_\mathrm{max}} \end{cases}, \tag{27}$$

$$\mathbf{y}_k^* = \begin{cases} \mathbf{C}_{11}\mathbf{x}_k^* + \mathbf{D}_{11}^*\bar{\mathbf{u}}_k + \mathbf{g}_{11}^\mathrm{c} & \text{if } (\mathbf{x}_k, \bar{\mathbf{u}}_k) \in \mathcal{P}_{11} \\ \vdots & \vdots \\ \mathbf{C}_{|\mathbf{M}_\mathrm{a}|s_\mathrm{max}}\mathbf{x}_k^* + \mathbf{D}_{|\mathbf{M}_\mathrm{a}|s_\mathrm{max}}^*\bar{\mathbf{u}}_k + \mathbf{g}_{|\mathbf{M}_\mathrm{a}|s_\mathrm{max}}^\mathrm{c} & \text{if } (\mathbf{x}_k^*, \bar{\mathbf{u}}_k) \in \mathcal{P}_{|\mathbf{M}_\mathrm{a}|s_\mathrm{max}} \end{cases}, \tag{28}$$

where

$$s_\mathrm{max} \triangleq \max_{i=1}^{|\mathbf{M}_\mathrm{a}|} s_i \tag{29}$$

denotes a maximal number of submodes over all the operating modes and $|\mathbf{M}_\mathrm{a}|$ is the cardinality of the set of allowed operating modes.

Remark. *Some rows of (27)-(28) can be omitted if for i^{th} operating mode there is only one PWA system mode or if the number of submodes s_i is lower than s_max. This full-size definition is useful for automated modes and submodes processing.*

Usually, the PWA systems are used to describe the behavior of a real system concerning different dynamics for different operating points. Here we extend the usage for decision system, which can optimize system energy consumption with compliance to references and system constraints.

The modes of PWA system here represent different control strategies or different system configurations (for example heat pump source/sink configuration; cooling/heating distinction for different systems; for HEV type of propulsion - petrol/-electric etc.).

Then we propose to use MPC for selection of system mode and thus values of binary and integral actuators and concurrently the control strategy of the continuously controlled actuators (set of controllers etc.).

MPC is employed to find which mode of system in (27)-(28) is optimal in terms of reference tracking, complying with the system constraints and power consumption minimization, all defined by cost function and model constraints. The cost function is used in the form

$$J_N(\mathbf{x}_0^*, \hat{\mathbf{u}}) = \sum_{k=0}^{N-1} \big[(\mathbf{x}_k^* - \mathbf{r}_k)^\intercal \mathbf{Q} (\mathbf{x}_k^* - \mathbf{r}_k) + \bar{\mathbf{u}}_k^\intercal \mathbf{R} \bar{\mathbf{u}}_k + \Delta\bar{\mathbf{u}}_k^\intercal \mathbf{S} \Delta\bar{\mathbf{u}}_k\big], \tag{30}$$

with $\mathbf{x}^*$ being the state vector, $\mathbf{r}$ the state references vector, $\bar{\mathbf{u}}$ the modified PWA system input vector and $\hat{\mathbf{u}}$ the vector of predicted inputs $\hat{\mathbf{u}} = \begin{bmatrix} \bar{\mathbf{u}}_k^\intercal & \bar{\mathbf{u}}_{k+1}^\intercal & \dots & \bar{\mathbf{u}}_{k+N-1}^\intercal \end{bmatrix}^\intercal$. The matrices $\mathbf{Q}$, $\mathbf{R}$, and $\mathbf{S}$ are the penalization matrices for state error, inputs, and input change rate. The matrices $\mathbf{R}$ and $\mathbf{S}$ contain element related to input $\tilde{u}$ on position [1,1]

$$\mathbf{R} = \begin{bmatrix} R_{11} & \dots \\ \vdots & \ddots \end{bmatrix}, \qquad \mathbf{S} = \begin{bmatrix} S_{11} & \dots \\ \vdots & \ddots \end{bmatrix} \tag{31}$$

and these elements can be used for influencing the mode switching. Firstly, if we sort the operating modes from best to worst (from any perspective), using R_{11} the mode selection can be adjusted. Secondly, the mode switching rate can be

penalized using S_{11}, which needs to be tuned to ensure the desired switching behavior.

Remark. *The cost function (30) is not used for optimizations in this form, as the PWA system (and also the penalization matrices) needs to be converted into MLD or LCP system to be usable with available solvers. However, the form of (30) is useful for its clearness and thus it is used for explanation of dummy input penalization.*

The result of cost function minimization is a vector of predicted optimal inputs $\hat{\mathbf{u}}$. If we consider standard receding horizon control (RHC) on prediction horizon N, the only first step inputs $\hat{\mathbf{u}}_k$ are applied on controlled system and the rest of predicted inputs ($\hat{\mathbf{u}}_{k+1} \dots \hat{\mathbf{u}}_{k+N-1}$) are discarded. We reuse this approach and extend it by discarding all the predicted inputs except $\tilde{u}_k$, which is used for operating mode selection.

The control of actuators is then managed by low-level algorithms, which ensure precise reference tracking, disturbance rejection, and other tasks. As this approach is aimed at a complex nonlinear system (tens of inputs, up to tens of thousands of states), the MPC cannot be solved for every existing input of the system.

We refer to this approach of high-level system modes selection as Decision Model Predictive Control (DMPC).

Remark. *The current inputs $\mathbf{u}_k^*$ could be also used for direct control of the system, but only if the system is simple enough. Another possibility is to use the inputs as high-level power inputs, e.g. to control the overall cooling/heating power of the heat pump system in a range of $\langle 0, 1 \rangle$, which is then realized by low-level control algorithms of compressor, expansion valve, fans, pumps, etc.*

IV. Example of DMPC for vehicle cabin heating

As an example, we introduce a simplified vehicle cabin, which is heated by a heat pump system with two different heat sources - ambient air and coolant (which ensures waste heat recovery from E-Drive and HV Battery).

A. Problem formulation

The simple vehicle cabin heat flows overview is in Fig. 1 with following symbol meanings: T_{cab} is the cabin temperature, T_{co} is the temperature of the coolant, TF is a Thermal Function, $\dot{Q}_{\text{c}}$ is thermal flow from HV compressor, $\dot{Q}_{\text{loss}}$ stands for thermal losses of the cabin, $\dot{Q}_{\text{amb}}$ is heat pump thermal flow from ambient to the cabin and $\dot{Q}_{\text{co}}$ is heat pump thermal flow from the coolant to the cabin.

Suppose we have two evaporators, which are connected into a refrigerant circuit in parallel. Each evaporator has its shut-off valve (SOV) marked as v_1 and v_2. The performance of the heat pump is controlled by compressor speed (u_{c}). Then we can write the simple model of cabin heating as

$$\mathbf{x}_{k+1} = \mathbf{f}(\mathbf{x}_k, \mathbf{u}_k) \tag{32}$$

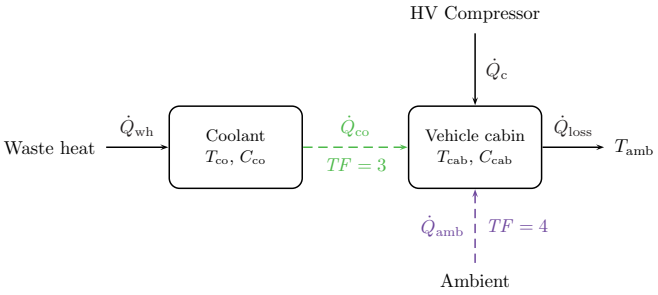

Fig. 1: Simple vehicle cabin heating

TABLE I: Estimated refrigeration system performance under different modes. CA - cooling with ambient air as a heat sink; CAT - CA with TES as an additional sink; HA - heating with ambient air as a heat source; HC - heating with coolant as a heat source.

	CA	CAT	HA	HC
p_{c} (Pa)	2 000 000	1 300 000	1 500 000	1 500 000
p_{e} (Pa)	350 000	350 000	150 000	250 000
COP $(-)$	1.633	2.864	2.28	2.816
P^{max} (W)	3869	2982	2310	2925
$\dot{Q}^{\text{max}}_{\text{cond}}$ (J s^{-1})	10 186	11 520	5268	8235
$\dot{Q}^{\text{max}}_{\text{evap}}$ (J s^{-1})	6318	8538	2958	5311

with

$$\mathbf{x} = \begin{bmatrix} T_{\text{cab}} & T_{\text{co}} \end{bmatrix}^{\intercal}, \qquad \mathbf{u} = \begin{bmatrix} v_1 & v_2 & u_c \end{bmatrix}^{\intercal}. \tag{33}$$

As there are two binary inputs (v_1 and v_2), all their possible combinations are

$$\mathbf{M} = \{00, 01, 10, 11\}, \tag{34}$$

but only two of them are allowed

$$\mathbf{M}_a = \{01, 10\}, \tag{35}$$

as both the SOV can not be closed or opened at the same time. Here we will violate the rule of denoting the PWA system modes from number 1, we will start from number 3 (as it is based on defined Thermal Function (TF)). So we mark the PWA system modes as TF 3 (heating with waste heat from coolant as a heat source) and TF 4 (heating with ambient air as a heat source).

Here we introduce the system constraints

$$273.15 - 20 < T_{\text{cab}} < 273.15 + 50 \quad \text{(K)}, \tag{36}$$
$$273.15 + 5 < T_{\text{co}} < 273.15 + 40 \quad \text{(K)}, \tag{37}$$
$$0 < u_{\text{c}} < 1 \quad (-), \tag{38}$$

which describe the polyhedron $\mathcal{P}$.

We present the modes of Vapor Compression Refrigeration System (VCRS), which are used within this example and also in Section V. The layout of complex VCRS is presented in Fig. 5 and it allows four main configurations, which are described in Tab. I and Fig. 2.

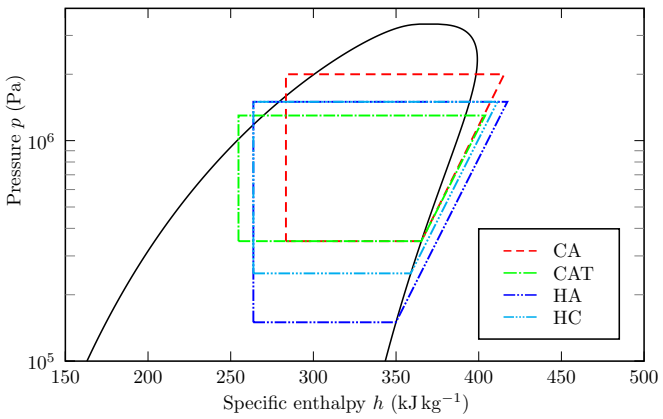

Fig. 2: Refrigeration system ph diagram for different modes. Abbreviations explained in the caption of Tab. I.

The overall discrete-time model of vehicle cabin heating with sampling period T_s is

$$\mathbf{x}_{k+1} = \begin{cases} \mathbf{A}\mathbf{x}_k + \mathbf{B}^*_{31}\bar{\mathbf{u}}_k + \mathbf{f}^\mathrm{c} & \text{if } TF = 3 \\ \mathbf{A}\mathbf{x}_k + \mathbf{B}^*_{41}\bar{\mathbf{u}}_k + \mathbf{f}^\mathrm{c} & \text{if } TF = 4 \end{cases}, \tag{39}$$

where

$$\mathbf{x} = \begin{bmatrix} T_\mathrm{cab} & T_\mathrm{co} \end{bmatrix}^\mathsf{T}, \qquad \bar{\mathbf{u}} = \begin{bmatrix} TF & u_\mathrm{c} \end{bmatrix}^\mathsf{T}, \tag{40}$$

$$\mathbf{A} = \begin{bmatrix} 1 - \frac{GT_\mathrm{s}}{C_\mathrm{cab}} & 0 \\ 0 & 1 \end{bmatrix}, \ \mathbf{B}^*_{31} = \begin{bmatrix} 0 & \frac{COP_\mathrm{HC} P^\mathrm{max}_\mathrm{HC} T_\mathrm{s}}{C_\mathrm{cab}} \\ 0 & -\frac{(COP_\mathrm{HC}-1) P^\mathrm{max}_\mathrm{HC} T_\mathrm{s}}{C_\mathrm{co}} \end{bmatrix}, \tag{41}$$

$$\mathbf{B}^*_{41} = \begin{bmatrix} 0 & \frac{COP_\mathrm{HA} P^\mathrm{max}_\mathrm{HA} T_\mathrm{s}}{C_\mathrm{cab}} \\ 0 & 0 \end{bmatrix}, \ \mathbf{f}^\mathrm{c} = \begin{bmatrix} \frac{GT_\mathrm{s}}{C_\mathrm{cab}} T_\mathrm{amb} \\ \frac{Q_\mathrm{wh} T_\mathrm{s}}{C_\mathrm{co}} \end{bmatrix}. \tag{42}$$

B. Results

This example was verified by simulation in MATLAB environment and the result is in Fig. 3. The MPC controller switches between TF 3 (heat pump with waste heat recovery) and TF 4 (heat pump with ambient air as a heat source) with satisfying the defined constraints (especially the coolant temperature) and the cabin temperature reference is also tracked successfully. This control problem could be also quite easily solved by some basic logic functions (or state diagram), but with increasing complexity (like VTMS in Fig. 5) it is not the preferable solution.

C. Energy consumption optimality

Since there is a penalty on compressor speed (and not directly on the compressor power consumption), we need to discuss energy optimality. We divide the discussion into two parts - cabin heat build-up and steady-state heating.

1) Cabin heat build-up: During cabin heat build-up the compressor will run at maximal speed and thus the resulting penalty of the compressor input u_c will be maximal for both the TF. The power consumption will be

$$P = \begin{cases} P^\mathrm{max}_\mathrm{HC} = 2925\,\mathrm{J\,s^{-1}} & \text{if } TF = 3 \\ P^\mathrm{max}_\mathrm{HA} = 2310\,\mathrm{J\,s^{-1}} & \text{if } TF = 4 \end{cases} \tag{43}$$

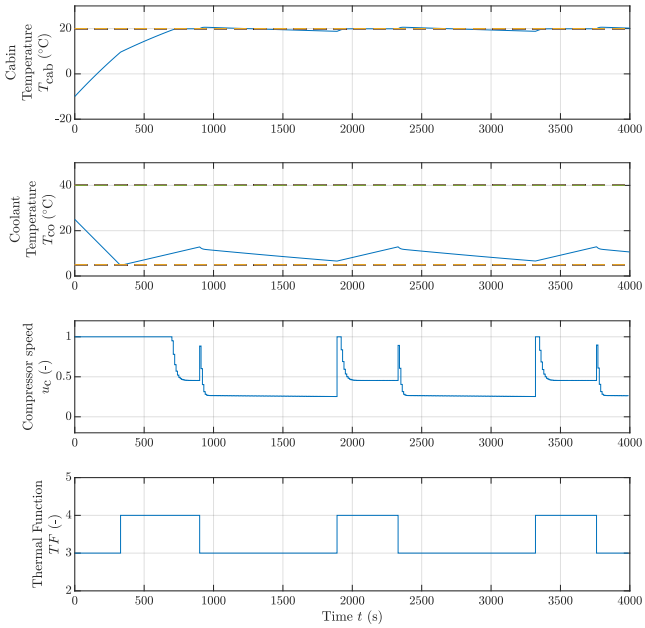

Fig. 3: Result of DMPC for simple vehicle cabin for $\dot{Q}_\mathrm{wh} = 1000\,\mathrm{W}$ and $T_\mathrm{amb} = -10\,°\mathrm{C}$

and overall heat flow rate into the cabin

$$\dot{Q}_\mathrm{cond} = \begin{cases} \dot{Q}^\mathrm{max}_\mathrm{cond,HC} = 8235\,\mathrm{J\,s^{-1}} & \text{if } TF = 3 \\ \dot{Q}^\mathrm{max}_\mathrm{cond,HA} = 5268\,\mathrm{J\,s^{-1}} & \text{if } TF = 4 \end{cases} \tag{44}$$

with

$$COP = \begin{cases} COP_\mathrm{HC} & = 2.82 \\ COP_\mathrm{HA} & = 2.28 \end{cases}. \tag{45}$$

1 J of heat supplied to cabin requires 0.35 W s and 0.44 W s of compressor power consumption for $TF = 3$ and $TF = 4$ respectively. Moreover for $TF = 3$ much higher thermal flow is available and thus faster control error decrease is possible (but limited by the amount of heat removed from coolant).

Thus the value of cost function will be dependent especially on the cabin temperature control error and the MPC will select the TF, which will provide faster control error decrease over the prediction horizon.

2) Steady-state heating: During steady-state heating, only heat losses to ambient need to be compensated by heat pump heating. Considering heat losses $\dot{Q}_\mathrm{loss} = 1500\,\mathrm{J\,s^{-1}}$, we need the same thermal flow rate $\dot{Q}_\mathrm{cond} = \dot{Q}_\mathrm{loss}$ from the heat pump to keep the cabin temperature at the defined reference.

During $TF = 3$, the maximal heat flow to cabin is $\dot{Q}^\mathrm{max}_\mathrm{cond,HC} = 8235\,\mathrm{J\,s^{-1}}$, leading to $u_\mathrm{c} = \frac{1500}{8235} = 0.182$ with electric power consumption $P = P^\mathrm{max}_\mathrm{HC} u_\mathrm{c} = 532.8\,\mathrm{W}$.

During $TF = 4$, the maximal heat flow to cabin is $\dot{Q}^\mathrm{max}_\mathrm{cond,HA} = 5268\,\mathrm{J\,s^{-1}}$, leading to $u_\mathrm{c} = \frac{1500}{5268} = 0.285$ with electric power consumption $P = P^\mathrm{max}_\mathrm{HA} u_\mathrm{c} = 657.7\,\mathrm{W}$.

In general, if we consider the same discharge (high side, head) pressure and different suction (low side) pressures (due to different cold reservoir temperatures), we can say that with

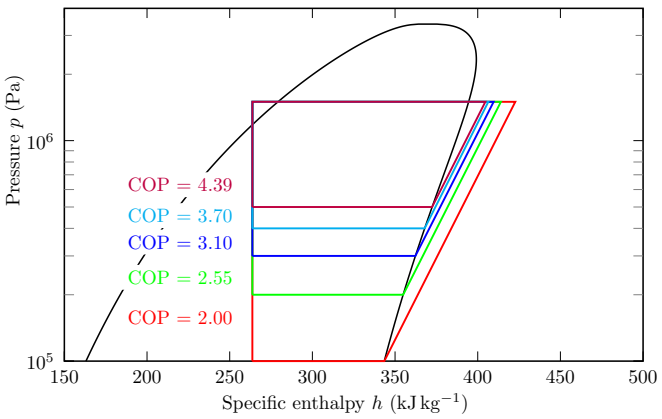

Fig. 4: ph diagram for different COP and suction pressures

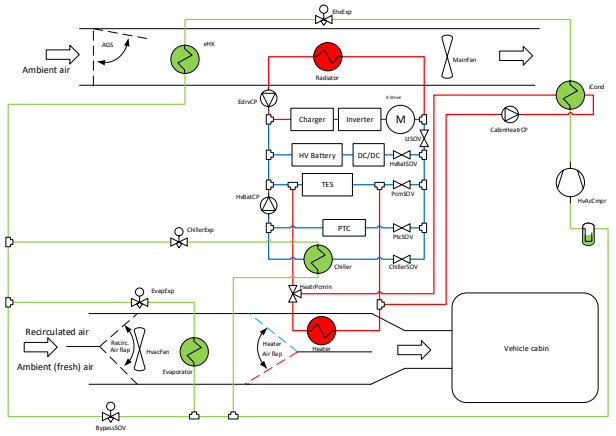

Fig. 5: VTMS for a fully electric vehicle from OSEM-EV project

increasing suction pressure the COP increases too (due to the shape of saturated vapor line). This is quite obvious, for the ideal reversible cycle we can write

$$COP = \frac{T_{\mathrm{H}}}{T_{\mathrm{H}} - T_{\mathrm{C}}}, \tag{46}$$

where T_{C} and T_{H} are cold and hot reservoirs temperatures respectively. The difference between temperatures determines the theoretical COP maximum, the smaller the difference, the higher the COP. The pressures are connected with the temperatures of the reservoirs (if we had a heat exchanger of infinite size, the saturated temperature would be the same as the reservoir temperature, otherwise there would be some thermal gradient). Equation (46) does not hold for real systems exactly, but the tendency is the same, as it is shown in Fig. 4 (includes isentropic efficiency).

We can write the current heat flow rate from the condenser as

$$\dot{Q}_{\mathrm{cond}} = \dot{m}\Delta h, \tag{47}$$

where $\dot{m}$ is the refrigerant mass flow rate in condenser and $\Delta h = h_{\mathrm{i}} - h_{\mathrm{o}}$ is condenser specific enthalpy difference with h_{i} and h_{o} being the condenser inlet and outlet specific enthalpy respectively. Now we neglect the changes of Δh (as the changes are negligible compared to mass flow rate changes: $11\,\%$ vs $470\,\%$ for suction pressures of $1\,\mathrm{bar}$ and $5\,\mathrm{bar}$; under constant compressor speed) and we will concentrate on changes within $\dot{m}$

$$\dot{m} = u_{\mathrm{c}} \frac{8000}{60} \rho V \eta_{\mathrm{vol}}, \tag{48}$$

where ρ is the refrigerant volumetric mass density at the compressor suction side, V is compressor displacement and η_{vol} is compressor volumetric efficiency.

Then to keep the heat flow from condenser constant, the refrigerant mass flow rate must be also constant and we can write

$$u_{\mathrm{c}} = \frac{1}{\rho} \frac{60\dot{m}}{8000 V \eta_{\mathrm{vol}}} \tag{49}$$

and it is obvious that with increasing refrigerant volumetric mass density ρ (caused by increasing suction pressure) the compressor speed input u_{c} is decreasing.

For minimal compressor speed u_{c} (decreases with increasing suction pressure) the COP is maximal (increases with increasing suction pressure) and thus for defined thermal flow to cabin $\dot{Q}_{\mathrm{cond}}$ the compressor power is

$$P = \frac{\dot{Q}_{\mathrm{cond}}}{COP} \tag{50}$$

and the compressor power is minimal for maximal possible COP. Then we can conclude that for the lowest possible compressor speed u_c (required to supply needed thermal flow to the cabin) the compressor power consumption will be the lowest possible and it is sufficient to penalize the compressor speed in MPC problem formulation to achieve an optimal (minimal) compressor power consumption with sufficient penalty on its speed.

V. DMPC for FEV VTMS

The vehicle thermal management system (VTMS) in Fig. 5 was divided into three subsystems - HVAC, HV Battery, and E-Drive. For each subsystem, several Thermal Functions (TF) were defined to allow the required functionality (heating or cooling of the subsystems). Then compatibility of TFs between subsystems was analyzed and a table of compatible TFs was created. Still there remained a lot of possible combinations (approx. 20-30), thus we assembled preferred combinations of TF for the subsystems and each combination is called Overall Thermal Function (OTF) and described by number (124, 211, 224, 373, 463, 511, 524). The first position denotes HVAC TF, the second stands for HV Battery TF and the third belongs to E-Drive TF.

The list of OTF is presented in Tab. II. Moreover there exist some submodes within these OTFs, like OTF 373e, which allows recovery of waste heat even if the TES is exhausted. Also, the OTF 124 was divided into multiple submodes to

TABLE II: Overall thermal functions overview

	HVAC	HV Battery	E-Drive
OTF 124	cooling by ambient air	cooling by ambient air	cooling by ambient air
OTF 211	cooling by VCRS with ambient air and TES as a heat sinks	cooling by VCRS with ambient air and TES as a heat sinks	cooling by ambient air
OTF 224	cooling by VCRS with ambient air and TES as a heat sinks	cooling by ambient air	cooling by ambient air
OTF 373	heating by VCRS with coolant as a heat source	cooling by coolant and VCRS	cooling by coolant and VCRS
OTF 463	heating by VCRS with ambient air as a heat source	cooling by coolant	cooling by coolant
OTF 511	cooling by VCRS with ambient air as a heat sink	cooling by VCRS with ambient air as a heat sink	cooling by ambient air
OTF 524	cooling by VCRS with ambient air as a heat sink	cooling by ambient air	cooling by ambient air

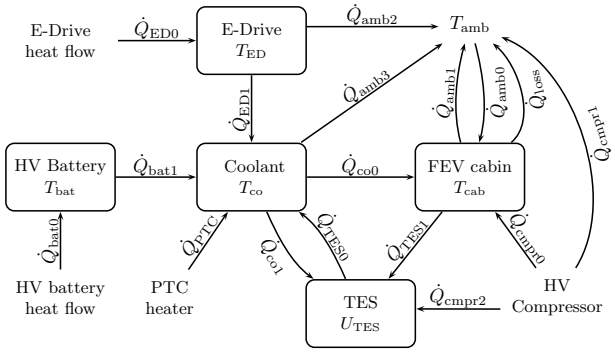

Fig. 6: Diagram of FEV simplified heat flows

ensure the appropriate behavior of the system model (the heat flow rate caused by cabin ventilation is significantly dependent on cabin air temperature).

1) VTMS PWA model: The model of VTMS energy flows was assembled in a general form as shown in Fig. 6 and it can be described by following set of equations

$$C_{\text{cab}}\frac{\mathrm{d}T_{\text{cab}}}{\mathrm{d}t} = \dot{Q}_{\text{amb0}} - \dot{Q}_{\text{loss}} - \dot{Q}_{\text{amb1}} + \dot{Q}_{\text{cmpr0}} - \dot{Q}_{\text{TES1}} + \dot{Q}_{\text{co0}}, \tag{51}$$

$$C_{\text{co}}\frac{\mathrm{d}T_{\text{co}}}{\mathrm{d}t} = -\dot{Q}_{\text{co0}} + \dot{Q}_{\text{TES0}} - \dot{Q}_{\text{co1}} + \dot{Q}_{\text{PTC}} - \dot{Q}_{\text{amb3}} + \dot{Q}_{\text{ED1}} + \dot{Q}_{\text{bat1}}, \tag{52}$$

$$C_{\text{bat}}\frac{\mathrm{d}T_{\text{bat}}}{\mathrm{d}t} = \dot{Q}_{\text{bat0}} - \dot{Q}_{\text{bat1}}, \tag{53}$$

$$C_{\text{ED}}\frac{\mathrm{d}T_{\text{ED}}}{\mathrm{d}t} = \dot{Q}_{\text{ED0}} - \dot{Q}_{\text{ED1}} - \dot{Q}_{\text{amb2}}, \tag{54}$$

$$\frac{\mathrm{d}U_{\text{TES}}}{\mathrm{d}t} = \dot{Q}_{\text{TES1}} - \dot{Q}_{\text{TES0}} + \dot{Q}_{\text{co1}} + \dot{Q}_{\text{cmpr2}}, \tag{55}$$

$$\frac{\mathrm{d}T_{\text{amb}}}{\mathrm{d}t} = 0, \tag{56}$$

$$y_{\text{cab}} = T_{\text{cab}}, \tag{57}$$

$$y_{\text{bat}} = T_{\text{bat}}, \tag{58}$$

and we assume that it can be simplified, discretized and written for every single OTF in the state-space form

$$\mathbf{x}^*_{k+1} = \mathbf{A}\mathbf{x}^*_k + \mathbf{B}^*\bar{\mathbf{u}}_k + \mathbf{f}^{\text{c}}, \tag{59}$$

$$\mathbf{y}^*_k = \mathbf{C}\mathbf{x}^*_k + \mathbf{D}^*\bar{\mathbf{u}}_k + \mathbf{g}^{\text{c}}, \tag{60}$$

where

$$\mathbf{x}^* = \begin{bmatrix} T_{\text{cab}} & T_{\text{co}} & T_{\text{bat}} & T_{\text{ED}} & U_{\text{TES}} & T_{\text{amb}} \end{bmatrix}^\intercal, \tag{61}$$

$$\bar{\mathbf{u}} = \begin{bmatrix} OTF & u_{\text{cmpr}} & u_{\text{hf}} & u_{\text{cc}} & u_{\text{cb}} & u_{\text{ptc}} \end{bmatrix}^\intercal, \tag{62}$$

$$\mathbf{y}^* = \begin{bmatrix} y_{\text{cab}} & y_{\text{bat}} \end{bmatrix}^\intercal. \tag{63}$$

For each operating mode (represented by OTF) a dynamic affine model with the common state, input, and output vector is being formulated by omitting and expressing the thermal flows taken from the general model. The derived models are not shown within this text due to space limitation, but the approach is very similar to the example in Section IV with reusing the constants from Tab. I.

Here we remind that the PWA model does not aspire to be the exact representation of VTMS, it only serves as a high-level approximation for decision purposes. Also, the control vector obtained from the MPC controller is discarded except the OTF indicator and the actuators need to be controlled by another set of low-level algorithms in the final implementation.

2) MPTDC implementation: MPTDC algorithms were tested only in simulations, as the demonstration vehicle was not finished yet. MPT toolbox [11] in combination with MATLAB and Simulink was used for hybrid MPC controller design, simulations and code generation. Also, Hybrid Toolbox [12] provides similar features and could be used for this purpose.

Firstly, Model in the Loop (MIL) simulations were performed with controllers in both the implicit and explicit form. MIL simulations were convenient in the early stages of controller development due to the fast cycle of deployment and verification.

Secondly, Software in the Loop (SIL) simulations were executed employing the generated C code of MPC controller in explicit form. This simulation was performed in MATLAB/Simulink environment.

Finally, the MPC algorithms were verified in Processor in the Loop (PIL) simulation. The generated code of controller was implemented into the Infineon AURIX Tricore TC299TF microcontroller unit (MCU), placed on AURIX Starter Kit TC299. The MCU contains three cores running at 300 MHz, 8 MB FLASH (4x2 MB), and 728 kB RAM. Due to FLASH memory limitation, it was possible to implement the MPC controller with up to prediction horizon $N = 3$ with a sampling time of 10 s. It should not be an issue to prolong the prediction horizon with specifically designed PCB incorporating MCU and a bigger amount of FLASH memory.

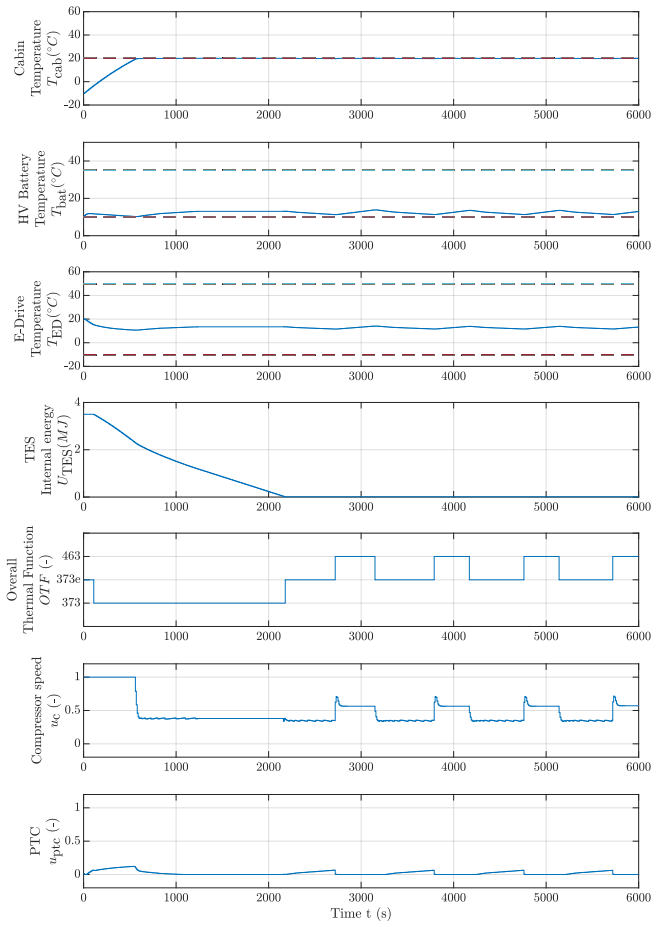

Fig. 7: MPTDC PIL simulation under winter condition with $T_{\mathrm{amb}} = -10\,^{\circ}\mathrm{C}$, $\dot{Q}_{\mathrm{ED0}} = 600\,\mathrm{W}$ and $\dot{Q}_{\mathrm{bat0}} = 400\,\mathrm{W}$

In Fig. 7 there is a PIL simulation result for winter vehicle operation. For the first approximately 2200 s, the OTF 373 is selected and waste heat and TES are fully utilized. After exhaustion of TES, the system switches between OTF 373e and 463, waste heat recovery function and heating with ambient air as a heat source respectively. The MPC algorithm selects the appropriate OTF based on constraints and references compliance.

It is noticeable that the PTC heater is occasionally requested to support the cabin heating by adding some heat to the coolant (power of up to 750 W). This helps to keep the system in the waste heat recovery mode (OTF 373 or 373e) and thus the overall power consumption is lower, than if the system falls into heat pump mode with ambient air as a heat source.

VI. Conclusion

In this paper, a model predictive control based decision algorithm was presented. It is useful for complex systems with binary or integer actuators, that can be modeled from a high-level perspective and the algorithm then can select the optimal operating mode.

This approach was demonstrated on an example of FEV simple cabin heating, where the algorithm was able to switch between two heat pump heat sources with fulfilling the constraints and following the cabin temperature reference.

The algorithm was applied to highly complicated VTMS for FEV and it was successfully implemented into automotive MCU Infineon AURIX Tricore TC299TF. Then the decision-making capabilities were presented within PIL simulation and the results are satisfactory.

There might be possibilities of improvements in terms of exported code size and future research could improve the usability of this approach. Moreover, it could be feasible to run the optimization in real-time (implicit or online MPC), which is not covered in this work. Successful MCU implementation of the B&B algorithm was reported in [13], thus real-time decision algorithm could also be the possible direction in this field.

Acknowledgment

This research was carried out under the project H2020 653514 OSEM-EV - Optimised and Systematic Energy Management in Electric Vehicles.

This research has been financially supported by the Ministry of Education, Youth and Sports of the Czech Republic under the project CEITEC 2020 (LQ1601).

References

[1] J. R. M. Delos Reyes, R. V. Parsons, and R. Hoemsen, "Winter Happens: The Effect of Ambient Temperature on the Travel Range of Electric Vehicles," *IEEE Transactions on Vehicular Technology*, vol. 65, pp. 4016–4022, June 2016.

[2] G. Mimberg and C. Massonet, "Battery concept to minimize the climate-related reduction of electric vehicles driving range," in *2017 12th International Conference on Ecological Vehicles and Renewable Energies, EVER 2017*, Institute of Electrical and Electronics Engineers Inc., May 2017.

[3] N. Meyer, I. Whittal, M. Christenson, and A. Loiselle-Lapointe, "The Impact of Driving Cycle and Climate on Electrical Consumption & Range of Fully Electric Passenger," in *EVS26 International Battery, Hybrid and Fuel Cell Electric Vehicle Symposium*, 2012.

[4] C. Gregor and R. V. Parsons, "Cold-weather modifications of plug-in hybrid electric vehicles for manitoba operation," in *2011 IEEE Electrical Power and Energy Conference, EPEC 2011*, pp. 421–425, 2011.

[5] Z. Zhang, J. Wang, X. Feng, L. Chang, Y. Chen, and X. Wang, "The solutions to electric vehicle air conditioning systems: A review," *Renewable and Sustainable Energy Reviews*, vol. 91, pp. 443–463, Aug. 2018.

[6] W. Heemels, B. De Schutter, and A. Bemporad, "Equivalence of hybrid dynamical models," *Automatica*, vol. 37, pp. 1085–1091, July 2001.

[7] M. Morari, "Hybrid system analysis and control via mixed integer optimization," *IFAC Proceedings Volumes*, vol. 34, pp. 1–12, June 2001.

[8] A. Bemporad and M. Morari, "Control of systems integrating logic, dynamics, and constraints," *Automatica*, vol. 35, pp. 407–427, Mar. 1999.

[9] E. Sontag, "Nonlinear regulation: The piecewise linear approach," *IEEE Transactions on Automatic Control*, vol. 26, pp. 346–358, Apr. 1981.

[10] F. Borrelli, M. Baotic, A. Bemporad, and M. Morari, "An efficient algorithm for computing the state feedback optimal control law for discrete time hybrid systems," in *Proceedings of the 2003 American Control Conference, 2003.*, vol. 6, pp. 4717–4722, IEEE, 2003.

[11] M. Herceg, M. Kvasnica, C. N. Jones, and M. Morari, "Multi-Parametric Toolbox 3.0," in *2013 European Control Conference (ECC)*, pp. 502–510, IEEE, July 2013.

[12] A. Bemporad, "Hybrid Toolbox - User's Guide." Available at: http://cse.lab.imtlucca.it/~bemporad/hybrid/toolbox, 2004.

[13] J. Novak and P. Chalupa, "Implementation of Mixed-integer Programming on Embedded System," *Procedia Engineering*, vol. 100, pp. 1649–1656, Jan. 2015.